Elastic Valve Using Induced-Charge Electro-Osmosis

Hideyuki Sugioka*

Frontier Research Center, Canon Inc. 30-2, Shimomaruko 3-chome, Ohta-ku, Tokyo 146-8501, Japan

(Received 9 November 2014; revised manuscript received 20 April 2015; published 2 June 2015)

Biomimic devices using induced-charge electro-osmosis (ICEO) is interesting since they have the possibility to realize high-performance functions with simple structures and with low-energy consumption. Thus, inspired by a cilium, we propose a two-dimensional artificial elastic valve using hydrodynamic force due to ICEO with a thin elastic beam in a microfluidic channel and numerically examine the valving performance. By an implicit strongly coupled simulation technique between a fluid and an elastic structure based on the boundary-element method, along with the thin-double-layer approximation, we realize stable calculations and find that the elastic valve using ICEO functions effectively at high frequency with low applied voltages in a realistic pressure flow. Further, we also examine passive motion of the valve; i.e., it stops a reverse flow effectively and releases a forward flow in the channel. We believe that our device can be used in a wide range of microfluidic applications, such as mixers, pumps, etc.

DOI: 10.1103/PhysRevApplied.3.064001

I. INTRODUCTION

Biomimic devices have much potential to obtain outstanding functions that ordinary machines cannot achieve. In particular, artificial cilia [1–4] have attracted much attention because of their large expectation to microfluidic applications [5], and the appearance of the artificial cilia is diverse [1]. For example, den Toonder *et al.* [6] experimentally reported that two-dimensional (2D) artificial cilia having a platelike but curled microbeam consisting of layers of polyimide and chromium can be driven by an electrokinetic force and generate substantial fluid flow and mixing in silicone oil. Shields *et al.* [2] also experimentally reported that artificial cilia made of rodlike polydimethylsiloxane containing dispersed superparamagnetic nanoparticles (Fe_3O_4) can be driven by a magnetic force and generate substantial fluid flow. Khaderi *et al.* [4] theoretically showed that the amount of fluid propelled is proportional to the area swept by the cilia by using a 2D explicit weakly coupled method between a fluid and an elastic beam based on the finite-element method. However, the magnetic cilia need large coils to produce strong magnetic fields, while the electrokinetic cilia in water have not been explored well at least theoretically because of their complexity in spite of their large potential for miniaturization and suitable circumstances for cells.

Recently, Bazant and Squires [7–9] showed that induced-charge electro-osmosis (ICEO), which includes ac electro-osmosis discovered by Ramos *et al.* [10,11], is a key concept for understanding the behaviors of metallic colloidal suspensions and flows around a metal post in a polarizable solution. ICEO is different from classical electro-osmosis because it is caused by the interaction between an electric field and ions in an electric double layer formed by the polarizing effect of the electric field; thus, it generates large flow velocity (approximately 1 mm/s) proportional to the applied electric field at low applied voltages (approximately 1 V), and it can be driven by ac electric fields. Therefore, the problems due to a dc electric field (such as a chemical reaction) can be avoided to some extent. Thus, in our previous papers [12,13], we propose a rotary microvalve that can move smoothly by using a slip velocity of ICEO on the surface in viscous-dominant circumstances, and it is important, since valves are dispensable elements in biomedical applications [5]. However, making the axis of rotation is a little difficult in smaller regions, although we believe it is still useful, and nature provides the solution as cilia in those regions.

Therefore, in this study, we focus on a cilialike 2D elastic valve using hydrodynamic force due to induced-charge electro-osmosis in water and elucidate its design concept. In particular, we consider the ICEO elastic valve having an oblique conductive beam that is connected directly to the lower electrode since such an asymmetrical high-ζ potential structure has not been explored well. Further, by using a newly developed implicit strongly coupled simulation method that solves both fluidic and elastic equations simultaneously (not alternately) based on the boundary-element method along with the thin-double-layer approximation, we report completely stable and mesh-free calculations. Here, the stable calculation means that the calculation does not magnify numerical errors during the time evolution.

II. THEORY

A. Geometry model

Figure 1 shows the schematic view of an elastic valve using ICEO. As shown in Fig. 1, we typically place a

*sugioka.hideyuki@canon.co.jp

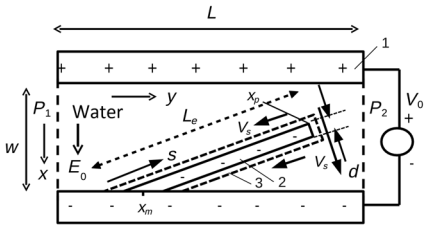

FIG. 1. Schematic view of an elastic valve using ICEO. 1: Pair of electrodes. 2: Conductive elastic beam. 3: Electro double layer. We place a conductive elastic beam of length $L_e = 1.5w$ and width $d = 0.04w$ on the lower electrode in a rectangular channel of length $L = 2.25w$ and width $w = 100$ μm at a 20° tilt angle θ. Here, typically, the applied voltage V_0 is 1.19 V, $y_m = 0.4w$, and the pressure difference ΔP $(\equiv P_2 - P_1)$ is -4 Pa. The Poisson ratio ν and shear modulus G of the elastic beam are 0.5 and 0.01 MPa, respectively, while the viscosity μ is 1 mPa s.

conductive elastic beam of length $L_e = 1.5w$ and width $d = 0.04w$ on the lower electrode in a rectangular channel of length $L = 2.25w$ and width $w = 100$ μm at a 20° tilt angle θ and apply an electric voltage V_0 $(= 1.19$ V) between the electrodes under the existence of the pressure difference ΔP $(\equiv P_2 - P_1)$ in water.

B. Numerical model

Numerically, we consider a 2D quasistatic Stokes flow without Brownian motion and a 2D quasistatic motion of the elastic beam; i.e., we consider the limit in which the Reynolds number Re tends to zero, and the Peclet number is infinite with the balance between the viscous and elastic forces at each time step without considering inertia effects because of small Re. Namely, we solve a 2D implicit strongly coupled calculation method that solves both the fluidic and elastic equations simultaneously by the boundary-element method (BEM) along with the thin-double-layer approximation. I.e., we calculate the flow fields and deflections of the beam by using the Stokes equations of a fluid and Navier's equations of a solid,

$$\mu\nabla^2\boldsymbol{v} - \boldsymbol{\nabla}p = \boldsymbol{0}, \qquad \boldsymbol{\nabla}\cdot\boldsymbol{v} = 0, \tag{1}$$

$$\boldsymbol{\nabla}\cdot\sigma_e = 0, \qquad \sigma_e = \mu_e[\boldsymbol{\nabla u} + (\boldsymbol{\nabla u})^T] + \lambda_e(\boldsymbol{\nabla}\cdot\boldsymbol{u})\boldsymbol{I}, \tag{2}$$

$$\boldsymbol{v} = \tilde{\boldsymbol{v}} + \boldsymbol{V}_s, \quad \text{on} \quad S_b^o, \tag{3}$$

$$\boldsymbol{f}_e(=\boldsymbol{f}_e{}' + \boldsymbol{f}^{\text{dep}}) = \boldsymbol{f}_f, \quad \text{on} \quad S_b^i, \tag{4}$$

where p is the pressure, μ (approximately 1 mPa s) is the viscosity, $\boldsymbol{v}$ is the velocity, σ_e is the stress tensor of the beam, $\boldsymbol{u}$ is the displacement, μ_e and λ_e are Lame's constants on a solid, S_b^o and S_b^i denote the surfaces defined as the outside and inside edges, respectively, of the double layer, $\tilde{\boldsymbol{v}}$ is the velocity on S_b^i, $\boldsymbol{V}_s$ is the slip velocity on S_b^o, $\boldsymbol{f}_e^{\text{dep}}$ is the surface traction due to the dielectrophoresis (DEP), $\boldsymbol{f}_e{}'$ is the surface traction due to the deflection of a solid, and $\boldsymbol{f}_e$ and $\boldsymbol{f}_f$ are the total surface traction vectors (defined by the opposite normal vectors) of the beam and fluid, respectively. Further, by solving the Laplace equation $(\nabla^2\phi = 0)$ under the condition that $\phi = V_0$ and $\phi = 0$ on the upper and lower electrodes, respectively, and $\boldsymbol{n}\cdot\boldsymbol{\nabla}\phi = 0$ on S_b^o, we obtain the slip velocity $\boldsymbol{V}_s$ on S_b^o at each time step on the basis of the Helmholtz-Smoluchowski formula:

$$\boldsymbol{V}_s = -\frac{\epsilon\zeta}{\mu}\boldsymbol{E}_s, \tag{5}$$

where $\boldsymbol{E}_s$ $(= -\boldsymbol{\nabla}\phi)$ is the tangential electric field, ϵ (approximately $80\epsilon_0$) is the dielectric permittivity of the solvent (typically water), ϵ_0 is the vacuum permittivity, ζ $(\equiv\phi_i - \phi_o)$ is the ζ potential, $\boldsymbol{n}$ is the surface normal unit vector, and ϕ_o and ϕ_i $(= 0)$ are the potentials at S_b^o and S_b^i, respectively. Furthermore, we obtain the DEP traction due to the Maxwell stress as

$$\boldsymbol{f}^{\text{dep}} = -\frac{1}{2}\epsilon\boldsymbol{E}_s^2\boldsymbol{n}. \tag{6}$$

Please note that in many papers (e.g., in Refs. [14–17]), we can find the boundary equations of the fluid and solid corresponding to Eqs. (1) and (2) separately, and they are very similar expressions. Thus, we obtain the similar matrix formulations that $[H_f]\{\boldsymbol{v}\} + [G_f]\{\boldsymbol{f}_f\} = 0$ and $[H_e]\{\boldsymbol{u}\} + [G_f]\{\boldsymbol{f}_e\} = 0$, where [] denotes a matrix, {} denotes a column vector, and $\{\boldsymbol{v}\}$ and $\{\boldsymbol{f}_f\}$ [$\{\boldsymbol{u}\}$ and $\{\boldsymbol{f}_e\}$] are node vectors of the velocity and traction of fluid [displacement and traction of solid], respectively. Therefore, by considering $\{\boldsymbol{u}^{t=t_0+\Delta t}\} = \{\boldsymbol{u}^{t_0}\} + \Delta t\{\tilde{\boldsymbol{v}}^{t=t_0+\Delta t}\}$ with the boundary conditions of Eqs. (3) and (4), we obtain the unified matrix expression $[A]\{\boldsymbol{x}'\} = \{b\}$, where $\{\boldsymbol{x}'\}$ is an unknown vector consisting of unknown node traction and velocity vectors of a fluid at $t = t_0 + \Delta t$. Here, Δt denotes a time-step interval, and t_0 is arbitrary time. Similarly, the Laplace equation $(\nabla^2\phi = 0)$ also can be written in the matrix form; i.e., for the problem of ϕ_o, we obtain that $[H_p]\{\phi_o\} + [G_p]\{E_{n,o}\} = 0$, where $\{\phi_o\}$ and $\{E_{n,o}\}$ are node vectors of the potential and electric-field component perpendicular to the surface, respectively. Thus, by using Eq. (5) with the relation that $\boldsymbol{E}_s = -\boldsymbol{\nabla}\phi_o$ and $\zeta = \phi_i - \phi_o = -\phi_o$ at the beam surface, we obtain $\boldsymbol{V}_s$. Please note that specific forms of $[H_p]$ and $[G_p]$ also can be found in the standard textbooks for the boundary-element method, and sometimes we can use a fluidic solver for the Stokes equation as an electric potential solver for the Laplace equation by setting $\boldsymbol{\nabla}p = \boldsymbol{0}$.

C. Simple model of the ICEO elastic valve

From the viewpoint of engineering, even the simplest model is useful as a first step. Namely, by considering a slender-body limit as half of an elliptical particle with the Lorentz reciprocal theorem [14,18], we approximate the torque due to an ICEO flow as

$$\boldsymbol{T}^{\mathrm{ICEO}} \simeq -\frac{\mu}{L_e d}\int_{s=L_e}^{s=L_e+d}(\boldsymbol{n}\cdot\boldsymbol{r})(\boldsymbol{r}\times\boldsymbol{V}_s)ds \simeq -\frac{\mu}{L_e d}L_e^2 V_s^{\mathrm{edge}} d(-\boldsymbol{k}) \simeq \mu L_e V_s^{\mathrm{edge}}\boldsymbol{k}, \quad (7)$$

where $\boldsymbol{r}=\boldsymbol{x}-\boldsymbol{x}_m$, $\boldsymbol{x}_m$ is the position $(1, y_m)$, and $\boldsymbol{k}$ is a unit vector in the direction of z; thus, the equivalent concentrated force at $\boldsymbol{x}_p$ due to ICEO in the upper direction of the beam is approximated as

$$F^{*,\mathrm{ICEO}} \simeq \mu V_s^{\mathrm{edge}}. \quad (8)$$

Please note that we consider only the edge slip velocity V_s^{edge} as a dominant factor, and we approximate that $V_s^{\mathrm{edge}} \simeq c_e U_w$, where $U_w = \epsilon w E_0^2/\mu$ is a characteristic velocity of ICEO of the channel, and c_e is a shape factor related to the concentration of electric fields; here, $c_e \simeq 3$ from the results of our calculations [in Fig. 3(c)].

Further, by considering a simple fluidic resistor model in a Poiseuille flow, we approximate the pressure drop in the valve region as

$$\Delta P_v \simeq \frac{R_v}{R_V + R_o}\Delta P = \frac{1}{1+R_o/R_v}\Delta P, \quad (9)$$

where $R_v = 12\mu L_e\cos\theta/(w - L_e\sin\theta)^3$, $R_o = 12\mu(L - L_e\cos\theta)/w^3$, and $R_o/R_v = [(L/L_e\cos\theta) - 1](1 - L_e\sin\theta/w)^3$. Thus, we can approximate the torque due to the pressure difference as

$$T^{\Delta P}(\equiv L_e F^{*,\Delta P}) \simeq \int_{s=0}^{L_e}\left(1-\frac{s}{L_e}\right)\Delta P_v s\sin^2\theta ds \simeq \frac{1}{6}\Delta P_v L_e^2\sin^2\theta, \quad (10)$$

where $F^{*,\Delta P}$ is the equivalent concentrated force due to ΔP at the edge, and $[1-(s/L_e)]\Delta P_v\sin^2\theta ds$ is the local force perpendicular to the beam at s $(0 \le s \le L_e)$. Thus, we obtain $F^{*,\Delta P} \simeq \frac{1}{6}\Delta P_v L_e\sin^2\theta$. Here, we assume that a triangle zone under the beam is so-called dead water, and in this zone, the pressure is approximately constant; thus, we can approximate that the parallel force exerted on the beam changes linearly from $\Delta P_v\sin\theta ds$ at the beam bottom to zero at the beam edge, as a first approach. Furthermore, as for the pressure force, we cannot neglect the effect of the deflection of the beam (δ^{beam}), and by considering a projection length of the beam to the x axis in the deflection state, $F^{*,\Delta P}$ should be rewritten as

$$F^{*,\Delta P} \simeq \frac{1}{6}\Delta P_v(L_e\sin\theta + \delta^{\mathrm{beam}}\cos\theta)\sin\theta. \quad (11)$$

Please note that we consider that $\frac{1}{6}\Delta P_v\sin\theta$ is the resistance coefficient for the projection length of the beam. Thus, from Eqs. (8) and (11), the total equivalent concentrated force at the edge is

$$\tilde{P} \equiv F^{*,\mathrm{ICEO}} + F^{*,\Delta P} = c_e\epsilon V_0^2/w + \frac{1}{6}\Delta P_v(L_e\sin\theta + \delta^{\mathrm{beam}}\cos\theta)\sin\theta. \quad (12)$$

By using the linear beam theory, we can approximate the deflection of the beam as

$$\delta^{\mathrm{beam}} \simeq \frac{\tilde{P}L_e^3}{3EI}, \quad (13)$$

where $E = 2G(1+\nu)$ is Young's modulus, and $I = d^3/12$ is the moment of the inertia for the rectangular cross section of the unit thickness. Therefore, from Eqs. (12) and (13), we obtain

$$\delta^{\mathrm{beam}} \simeq \frac{Ac_e\epsilon V_0^2/w + ABL_e\sin\theta}{1 - AB\cos\theta}, \quad (14)$$

where $A = L_e^3/3EI$ and $B = \frac{1}{6}\Delta P_v\sin\theta$. Here, we assume that ΔP_v is constant, for simplicity. Further,

$$x_p = w - L_e\sin\theta - \delta^{\mathrm{beam}}\cos\theta, \quad (15)$$

$$U_p = \frac{Q}{w} \simeq \frac{(w - L_e\sin\theta - \delta^{\mathrm{beam}}\cos\theta)^3}{12\mu L_e w\cos\theta}, \quad (16)$$

where Q is the volumetric flow rate. From the kinematic and geometrical conditions, the moving and closing conditions of the elastic valve are roughly estimated as $\tilde{P} = F^{*,\mathrm{ICEO}} + F^{*,\Delta P} > 0$ and $\delta^{\mathrm{beam}}\cos\theta \ge (w - L_e\sin\theta)$, respectively. Under the conditions of Fig. 2, we obtain $F^{*,\mathrm{ICEO}} = \mu c_e U_w = 30\ \mu\mathrm{N/m}$, $F^{*,\Delta P} = -10\ \mu\mathrm{N/m}$, $\tilde{P} = 20\ \mu\mathrm{N/m}$, $\delta^{\mathrm{beam}}\cos\theta/w = 0.53$, and $(w - L_e\sin\theta)/w = 0.49$; i.e., the moving and closing conditions are satisfied in our calculations. Thus, the results of our numerical calculations are reasonable.

III. RESULTS

A. Active closing motions

Figure 2 shows the closing motion of the elastic valve using ICEO under the conditions that $\Delta P = -4$ Pa, $V_0 = 1.19$ V, $\nu = 0.5$, and $G = 0.01$ M Pa (typical value of poly-urethane). As shown in Fig. 2(a), initially we observe the substantial Poiseuille flow, but it is suppressed largely by the deflection of the beam at $t/T_0 = 5$ ms as in Fig. 2(b). Finally, it is stopped at $t/T_0 = 30$, although the tangential flow around the beam due to an ICEO slip velocity remains as shown in Fig. 2(c). Here, $T_0 = 1$ ms. Please note that although we use T_0 and $U_c = w/T_0$ for the convenience in this paper, they are just units, and they are not the represented values for time and velocity. Figure 2(d)

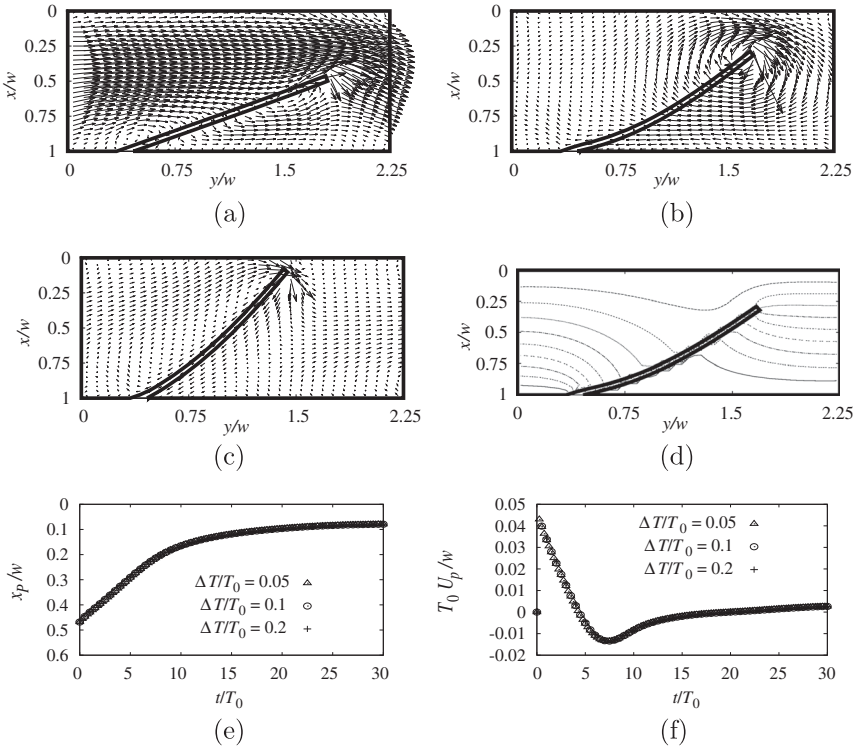

FIG. 2. Active closing motion of the ICEO elastic valve. Here, $L/w = 2.25$, $L_e/w = 1.5$, $d/w = 0.04$, $T_0\Delta P/\mu = -4$, $T_0 G/\mu = 10^4$, $\nu = 0.5$, and $T_0 U_w/w = 0.1$; e.g., $w = 100\ \mu$m, $T_0 = 1$ ms, $\mu = 1$ mPa s, $\Delta P = -4$ Pa, $G = 0.01$ MPa, and $V_0 = 1.19$ V. (a) Flow field at $t/T_0 = 0$. (b) Flow field at $t/T_0 = 5$. (c) Flow field at $t/T_0 = 30$. (d) Potential field at $t/T_0 = 5$. (e) Dependence of x_p on time. (f) Dependence of U_p on time.

shows a potential field at $t/T_0 = 5$, and it tells us clearly that the oblique structure connected to the lower electrodes gives the preferable large-ζ potential and large tangential electric field around the peak position ($\boldsymbol{x}_p$). This fact is an origin of the large slip velocity at the edge of the beam in the direction of the lower right. Because of this large slip velocity, the response time of the elastic valve becomes very short. Actually, as shown in Figs. 2(e) and 2(f), the response time of the peak position x_p and the average flow velocity U_p is approximately 5–10 ms; here, U_p is measured at $y = 0$. Further, the time-evolution curves of x_p and U_p are invariable under the condition that $\Delta t/T_0 = 0.05$, 0.1, and 0.2; it shows excellent stability of our calculations using the implicit strongly coupled method explained in Sec. II. Please note that in our trial, the explicit weakly coupled method that solves fluid and solid equations alternatively becomes unstable because of the high nonlinearity of an ICEO flow even for small Δt; i.e., although we need to neglect the variance of fluidic (elastic) surface traction during the step period Δt when we solve the solid (fluid) equations in the weakly coupled method, the sum of numerical errors increases rapidly. Thus, after several time steps, the matrix calculation becomes unable to converge even for small Δt.

Figure 3 shows detailed characteristics of the ICEO elastic valve. As shown in Figs. 3(a)–3(c), the ζ potential, tangential electric field, and slip velocity are very high at the edge of the elastic beam ($1.5 \le s \le 1.5 + d$) during the closing motion. In particular, the maximum ζ potential is comparable to the applied voltage ($\zeta^{\mathrm{edge}} \simeq V_0 \simeq 1.19$ V), and the maximum tangential electric field is several times the average electric field ($E_s \simeq 4E_0 \simeq 40$ kV/m); thus, the maximum slip velocity also becomes several times that of the ICEO characteristic flow velocity of the channel ($V_s^{\mathrm{edge}} \simeq 3U_w \simeq 30$ mm/s), where $U_w = \epsilon w E_0^2/\mu$. Please note that, roughly speaking, the value of V_s^{edge} is about 30 times higher than that of the ordinary ICEO characteristic flow velocity (approximately 1 mm/s). Further, Fig. 3(d) shows that the traction due to the DEP effects also has the maximum value at the edge, but it does not contribute largely to the deflection of the beam as shown in Fig. 3(e). Please note that in Fig. 3(e), the circles show the time evolution of the peak position considering DEP effects, while the triangles show the time evolution of the peak position not considering DEP effects. Furthermore, in Fig. 3(f), the square, circle, triangle, and cross show the time evolution of x_p at $\Delta P = -2$, -4, -8, and -16 Pa, respectively; thus, we find that the ICEO elastic valve works under the condition that $\Delta P \ge -4$ Pa at $V_0 = 1.19$ V.

Figure 4 shows the dependence of x_p on V_0 at $\Delta P = 0$ with the various parameters. As shown in Fig. 4, the value of x_p approaches zero as V_0 increases under the condition that $L_e \ge 1.5w$, $\theta \ge 20°$, and $d \le 0.08w$. It simply means that to close a valve at suitable applied voltages, the stiffness of the oblique beam should be weak enough to deflect. Further, in Fig. 4, the numerical results agree fairly well with those of the simple model described by Eq. (15)

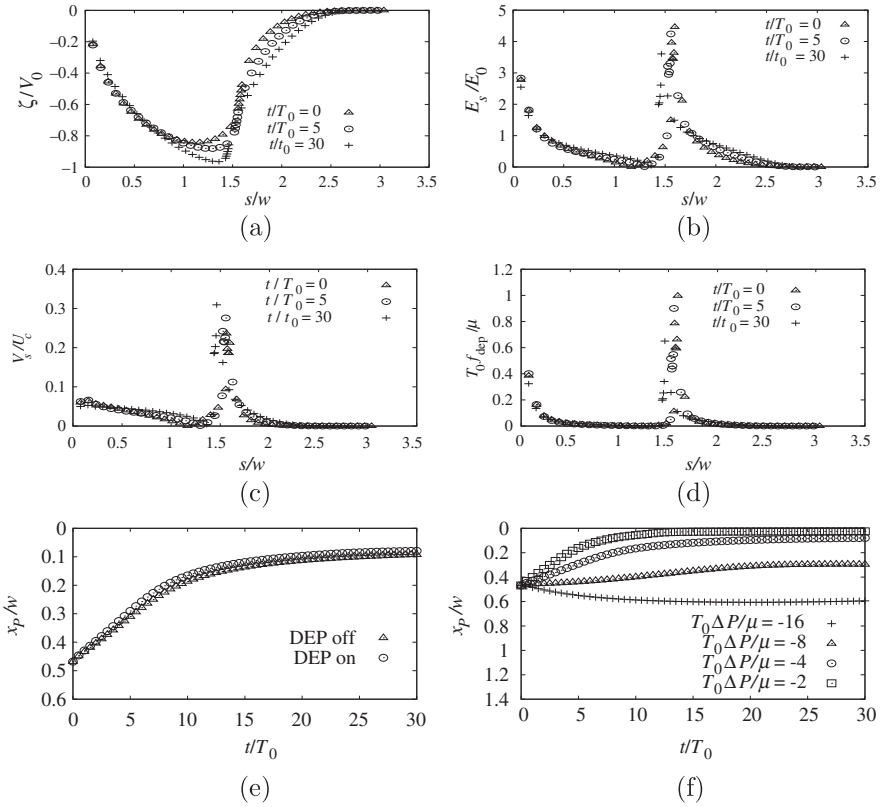

FIG. 3. Characteristics of the ICEO elastic valve during an active closing motion. Here, $U_c = w/T_0$, $L/w = 2.25$, $L_e/w = 1.5$, $d/w = 0.04$, $T_0\Delta P/\mu = -4$, $\nu = 0.5$, $T_0 G/\mu = 10^4$, and $T_0 U_w/w = 0.1$; e.g., $w = 100\ \mu$m, $T_0 = 1$ ms, $U_c = 0.1$ m/s, $\mu = 1$ mPa s, $\Delta P = -4$ Pa, $G = 0.01$ MPa, and $V_0 = 1.19$ V. In (e), the circle and triangle show the time evolution of x_p in the cases that consider and do not consider the DEP effect, respectively. In (f), the square, circle, triangle, and cross show the time evolution of x_p at $T_0\Delta P/\mu = -2$, -4, -8, and -16, respectively. (a) ζ vs s. (b) E_s vs s. (c) V_s vs s. (d) f_{def} vs s. (e) x_p vs t. (f) x_p vs t.

at small applied voltages ($V_0 < 0.3$), although there is much discrepancy between the analytical and numerical values under the condition that $G \geq 20$ kPa, $d/w \geq 0.08$, and $V_0 > 0.7$ V. Thus, we can rely on the simple model to some extent at $\Delta P = 0$ for small applied voltages.

Figures 5(a)–5(d) show the dependence of x_p on L_e, θ, G, and d, respectively, at $V_0 = 0.3$ V and $\Delta P = 0$. As shown in Fig. 5, the tendency of the numerical results agrees fairly well with that of the results of the simple model described by Eq. (15). Further, in Fig. 5, the broken lines show the initial positions at $V_0 = 0$ V and $\Delta P = 0$ Pa; thus, we can see the gap length of the channel and the deflection of the beam at the same time. In particular, from Eq. 5(b), we find that the dependence of

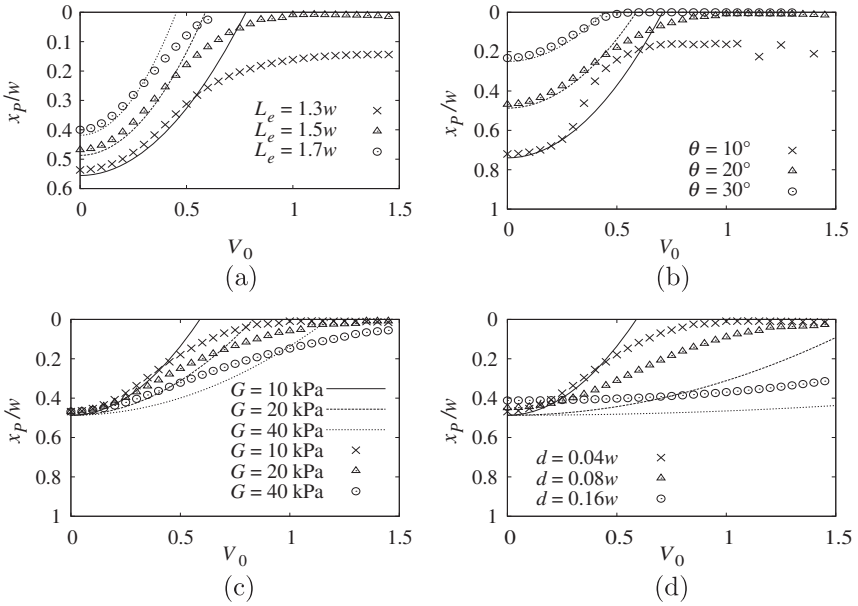

FIG. 4. Steady peak positions for active closing motions at $T_0\Delta P/\mu = 0$. Here, the set of standard parameters is $L/w = 2.25$, $L_e/w = 1.5$, $d/w = 0.04$, $\nu = 0.5$, and $T_0 G/\mu = 10^4$; e.g., $w = 100\,\mu$m, $T_0 = 1$ ms, $\mu = 1$ mPa s, and $G = 0.01$ MPa. The solid, broken, and dotted lines show the analytical results at $L_e/w = 1.3$, 1.5, and 1.7 in (a) [at $\theta = 10°$, 20°, and 30° in (b), at $G = 10$, 20, and 40 kPa in (c), and at $d = 0.04$, 0.08, and 0.16 kPa in (d)], respectively. (a) Dependence of x_p on V_0. (b) Dependence of x_p on V_0. (c) Dependence of x_p on V_0. (d) Dependence of x_p on V_0.

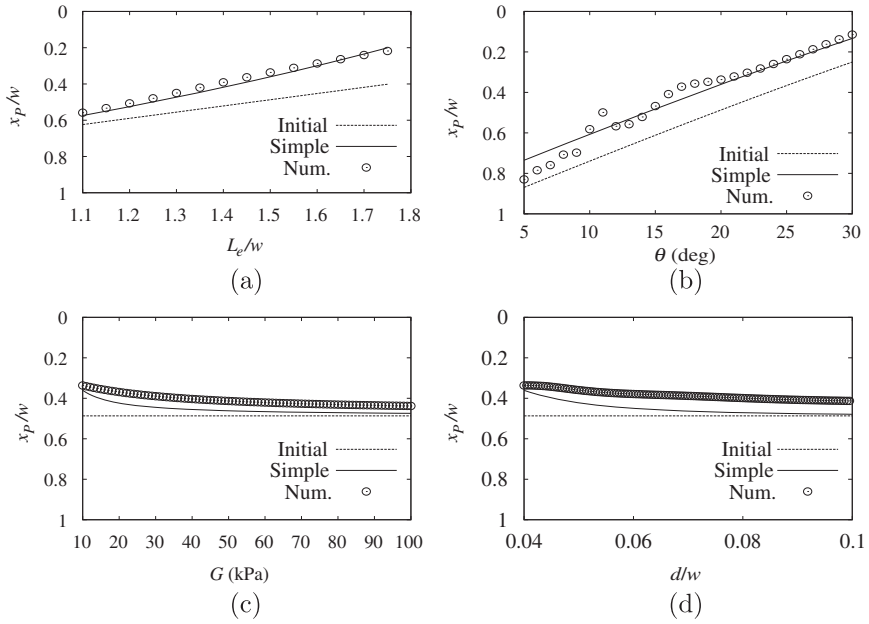

FIG. 5. Steady peak positions for active closing motions at $V_0 = 0.3$ V and $T_0\Delta P/\mu = 0$. Here, the set of standard parameters is $L/w = 2.25$, $L_e/w = 1.5$, $d/w = 0.04$, $\nu = 0.5$, and $T_0G/\mu = 10^4$; e.g., $w = 100$ μm, $T_0 = 1$ ms, $\mu = 1$ mPa s, and $G = 0.01$ MPa. Circles show the numerical results for the steady states, while solid and broken lines show the analytical result of the simple model for the steady and initial states, respectively. (a) Dependence of x_p on L_e. (b) Dependence of x_p on θ. (c) Dependence of x_p on G. (d) Dependence of x_p on d.

δ^{beam} on θ is more complex than that of the simple model at $\theta < 20°$.

Figure 6 shows steady peak positions x_p and the corresponding average flow velocities U_p for active motions. In Figs. 6(a) and 6(c) [in 6(b) and 6(d)], solid, broken, and dotted lines show the results of the simple model at $T_0\Delta P/\mu = 0$, -2, and -4 (at $V_0 = 0$, 0.99, and 1.19), respectively. As shown in Fig. 6, since the problem is a highly complicated nonlinear problem, the analytical and numerical results are not in agreement with each other at $V_0 \geq 0.99$ V and at $T_0\Delta p/\mu \leq -2$; however, both the numerical and analytical results show that the open states of the valve at $T_0\Delta P/\mu = 0$, -2, and -4 (at $V_0 = 0$, 0.99, and 1.19) can be switched to the closed states by increasing the applied voltage (pressure). Thus, the simple model is still important as the first estimation for the ICEO elastic valves.

B. Passive opening and closing motions

Figure 7 shows a passive opening motion for a forward pressure flow. As shown in Figs. 7(a) and 7(b), the forward pressure flow at $\Delta P = -4$ Pa deflects the beam in the lower direction and releases the flow more. Further, Figs. 7(c) and 7(d) [Figs. 7(e) and 7(f)] show the

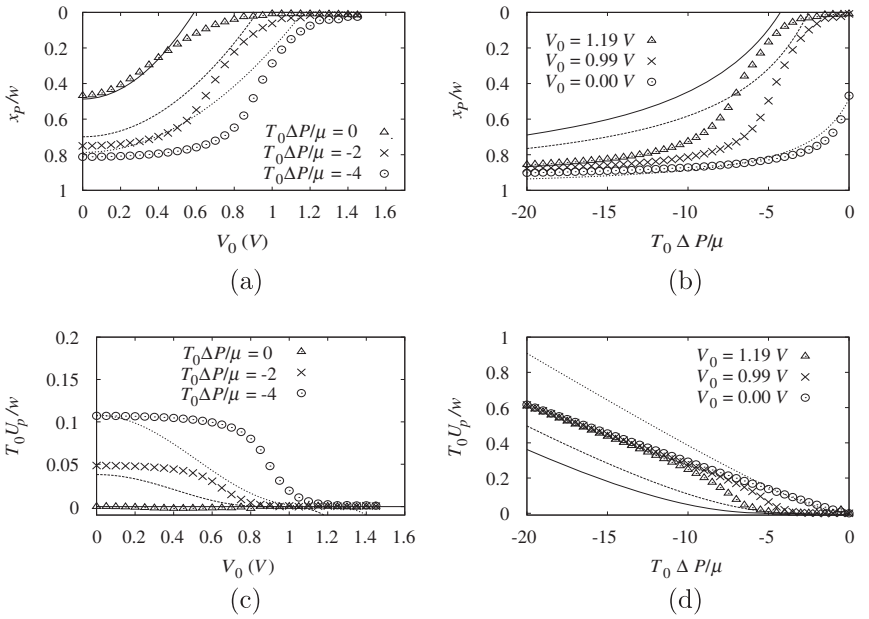

FIG. 6. Steady peak positions and the corresponding average flow velocities for the active closing motions. Here, the set of standard parameters is $L/w = 2.25$, $L_e/w = 1.5$, $d/w = 0.04$, $\nu = 0.5$, and $T_0G/\mu = 10^4$; e.g., $w = 100$ μm, $T_0 = 1$ ms, $\mu = 1$ mPa s, and $G = 0.01$ MPa. In (a),(c) [in (b),(d)], the solid, broken, and dotted lines show the results of the simple model at $T_0\Delta P/\mu = 0$, -2, and -4 (at $V_0 = 0$, 0.99, and 1.19), respectively. (a) Dependence of x_p on V_0. (b) Dependence of x_p on ΔP. (c) Dependence of U_p on V_0. (d) Dependence of U_p on ΔP.

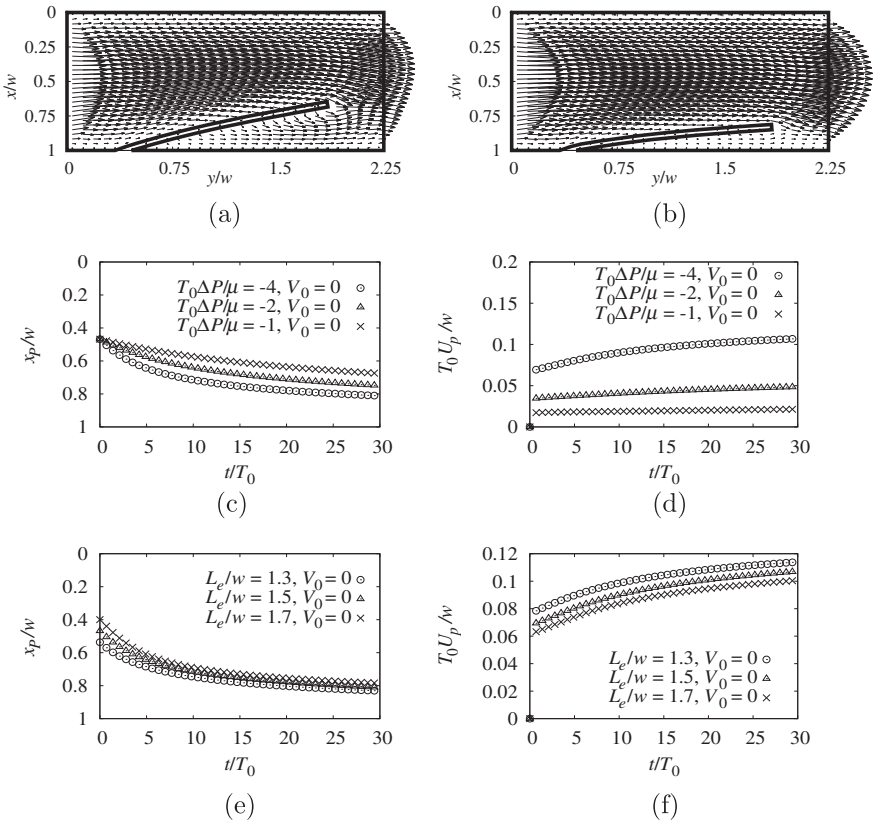

FIG. 7. Passive opening motion for a forward pressure flow. Here, $L/w = 2.25$, $L_e/w = 1.5$, $d/w = 0.04$, $\nu = 0.5$, $T_0G/\mu = 10^4$, and $T_0U_w/w = 0$; e.g., $w = 100\ \mu$m, $T_0 = 1$ ms, $\mu = 1$ mPa s, $G = 0.01$ MPa, and $V_0 = 0$ V. (a) Opening motion for a forward flow ($t/T_0 = 5$, $T_0\Delta P/\mu = -4$, $L_e/w = 1.5$). (b) Opening motion for a forward flow ($t/T_0 = 30$, $T_0\Delta P/\mu = -4$, $L_e/w = 1.5$). (c) Dependence of x_p on time ($L_e/w = 1.5$). (d) Dependence of U_p on time ($L_e/w = 1.5$). (e) Dependence of x_p on time ($T_0\Delta P/\mu = -4$). (f) Dependence of U_p on time ($T_0\Delta P/\mu = -4$).

dependence of x_p and U_p on time, respectively, at $T_0\Delta P/\mu = -4$, -2, and -1 [at $L_e/w = 1.3$, 1.5, and 1.7] during the passive opening motion. As shown in Figs. 7(c) and 7(d), the response time of the passive motions at $\Delta P = -4$ Pa is about 20 ms, and it is preferably short.

Figure 8 shows a passive closing motion for a reverse pressure flow. As shown in Figs. 8(a) and 8(b), the reverse

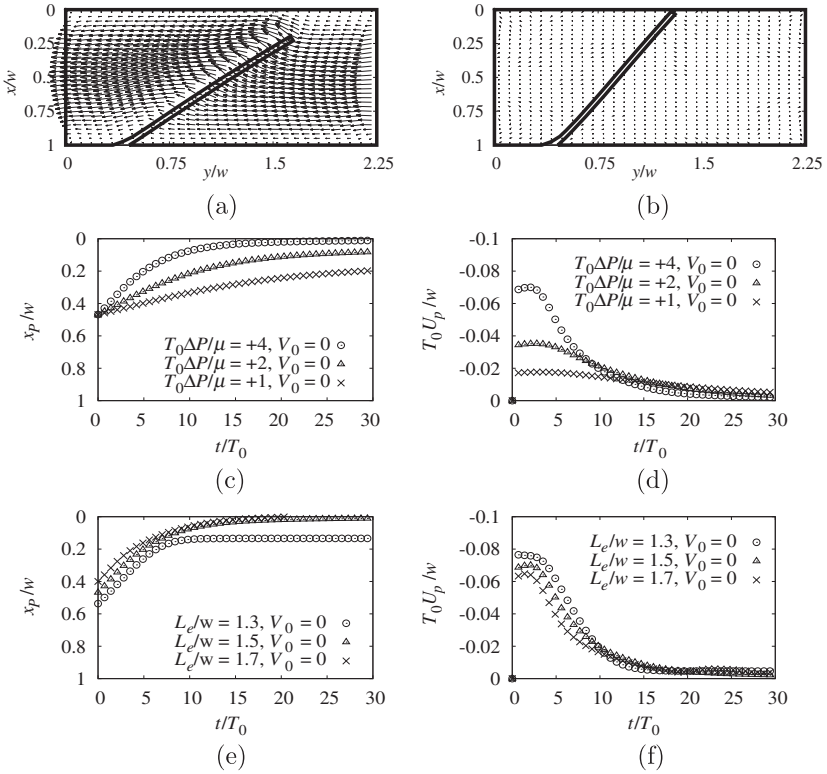

FIG. 8. Passive closing motion for a reverse pressure flow. Here, $L/w = 2.25$, $L_e/w = 1.5$, $d/w = 0.04$, $\nu = 0.5$, $T_0G/\mu = 10^4$, and $T_0U_w/w = 0$; e.g., $w = 100\ \mu$m, $T_0 = 1$ ms, $\mu = 1$ mPa s, $G = 0.01$ MPa, and $V_0 = 0$ V. (a) Closing motion for a reverse flow ($t/T_0 = 5$, $T_0\Delta P/\mu = +4$, $L_e/w = 1.5$). (b) Closing motion for a reverse flow ($t/T_0 = 30$, $T_0\Delta P/\mu = +4$, $L_e/w = 1.5$). (c) Dependence of x_p on time ($L_e/w = 1.5$). (d) Dependence of U_p on time ($L_e/w = 1.5$). (e) Dependence of xp on time ($T_0\Delta P/\mu = +4$). (f) Dependence of U_p on time ($T_0\Delta P/\mu = +4$).

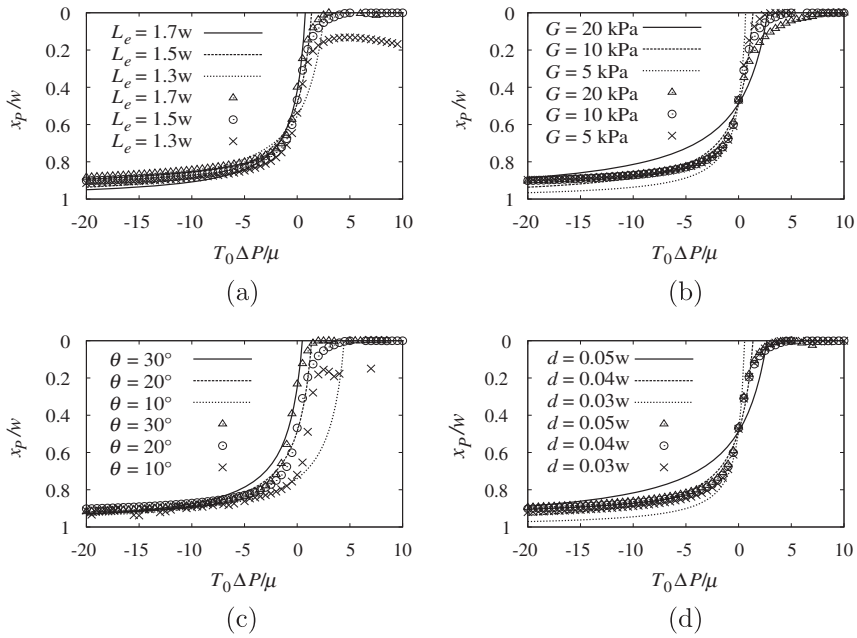

FIG. 9. Steady peak positions for passive motions at $V_0 = 0$ V. Here, the characters show the results of numerical calculations using the BEM; the lines show the result of the simple model. The set of standard parameters is $L/w = 2.25$, $L_e/w = 1.5$, $d/w = 0.04$, $\nu = 0.5$, $T_0G/\mu = 10^4$, and $T_0U_w/w = 0$; e.g., $w = 100$ μm, $T_0 = 1$ ms, $\mu = 1$ mPa s, and $G = 0.01$ MPa. (a) Dependence of x_p on ΔP ($V_0 = 0$ V). (b) Dependence of x_p on ΔP ($V_0 = 0$ V). (c) Dependence of x_p on ΔP ($V_0 = 0$ V). (d) Dependence of x_p on ΔP ($V_0 = 0$ V).

pressure flow at $T_0\Delta P/\mu = +4$ deflects the beam in the upper direction and stops the flow. Further, Figs. 8(c) and 8(d) [Figs. 8(e) and 8(f)] show the dependence of x_p and U_p on time, respectively, at $T_0\Delta P/\mu = +4$, $+2$, and $+1$ [at $L_e/w = 1.3$, 1.5, and 1.7] during the passive motions. As shown in Figs. 8(c) and 8(d), the response time of the passive closing motion at $T_0\Delta P/\mu = +4$ is about 10 ms, and it is also preferably short.

Figure 9 (Fig. 10) shows the dependence of x_p (U_p) on ΔP for the steady state of the passive motions at $V_0 = 0$ V. As shown in Fig. 9, the passive elastic valve can be closed completely under the condition that $L_e/w \geq 1.5$ and $\theta \geq 20°$. This is because a too large deflection is required to close completely at $\theta = 10°$ and $L_e/w = 1.3$. Further, in Figs. 9 and 10, the peak position slowly approaches the constant value, and the corresponding average velocity increases almost linearly, approximately in the range $T_0\Delta P/\mu \leq -4$. Furthermore, the values of x_p and U_p agree fairly well between the numerical and analytical results approximately in the range $T_0\Delta P/\mu \leq +1$, as shown in Figs. 9 and 10.

Figures 11(a)–11(d) show the dependence of x_p on L_e, θ, G, and d, respectively, at $V_0 = 0$ V and $T_0\Delta P/\mu = -2$. As shown in Fig. 1, the tendency of the numerical results agrees fairly well with that of the results of the simple model described by Eq. (15). Further, in Fig. 11, broken lines show the initial positions at $V_0 = 0$ V and

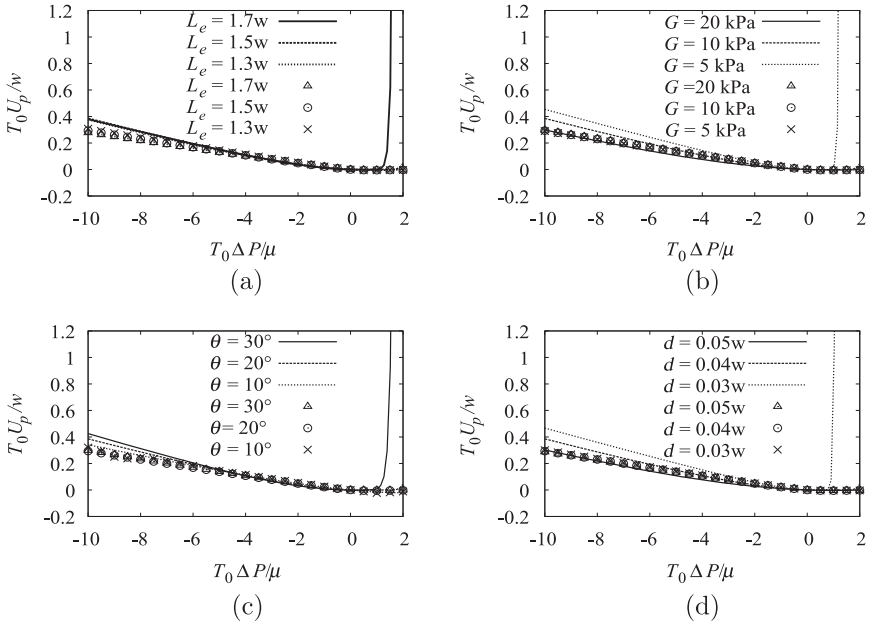

FIG. 10. Average flow velocity of the passive valve at $V_0 = 0$ V. Here, the characters show the results of numerical calculations using the BEM, while the lines show the result of the simple model. The set of standard parameters is $L/w = 2.25$, $L_e/w = 1.5$, $d/w = 0.04$, $\nu = 0.5$, $T_0G/\mu = 10^4$, and $T_0U_w/w = 0$; e.g., $w = 100$ μm, $T_0 = 1$ ms, $\mu = 1$ mPa s, and $G = 0.01$ MPa. (a) Dependence of U_p on ΔP ($V_0 = 0$ V). (b) Dependence of U_p on ΔP ($V_0 = 0$ V). (c) Dependence of U_p on ΔP ($V_0 = 0$ V). (d) Dependence of U_p on ΔP ($V_0 = 0$ V).

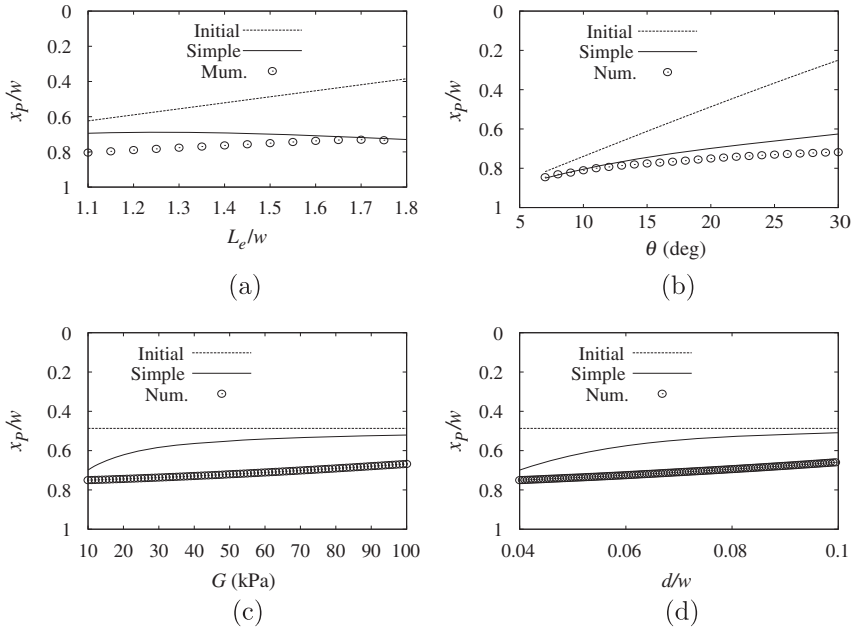

FIG. 11. Steady peak positions for passive opening motions at $V_0 = 0$ V and $T_0\Delta P/\mu = -2$. Here, the set of standard parameters is $L/w = 2.25$, $L_e/w = 1.5$, $d/w = 0.04$, $\nu = 0.5$, and $T_0 G/\mu = 10^4$; e.g., $w = 100$ μm, $T_0 = 1$ ms, $\mu = 1$ mPa s, and $G = 0.01$ MPa. The circles show the numerical results for the steady states, while the solid and broken lines show the analytical result of the simple model for the steady and initial states, respectively. (a) Dependence of x_p on L_e. (b) Dependence of x_p on θ. (c) Dependence of x_p on G. (d) Dependence of x_p on d.

$\Delta P = 0$ Pa. As shown in Figs. 11(a) and 11(b), the initial positions approach the upper electrode as the values of L_e and θ increase; however, because of the passive opening motions due to the forward flow, the steady opening positions are approximately constant. Thus, the value condition of L_e and θ (e.g., $L_e \geq 1.5$ and $\theta \geq 20°$) is preferable for the valve design.

IV. DISCUSSION

A. The meaning of the ICEO elastic valve

Although the analysis of a conductive membrane that considers an ICEO flow exists [19], the cilialike ICEO elastic valve is first proposed and examined theoretically in this paper. Further, different from the magnetic cilia by Shields *et al.* [2] and the 2D electrokinetic cilia by den Toonder *et al.* [6], the ICEO elastic valve works at low voltages ($V_0 \sim 1$ V) in water and with a high response time ($t_r^{\text{ICEO elastic valve}} \sim 5$–$10$ ms) without large equipment. Thus, it is promising for various biomedical applications. In addition, the active closing time of the ICEO elastic valve is approximately 1.5 to 3 times higher than that of the ICEO rotary valve ($t_r^{\text{ICEO rotary valve}} = 16$ ms) [12] under the same condition that $\Delta P = -4$ Pa, $V_0 = 1.19$ V, and $w = 100$ μm, although from Eqs. (11) and (12) we can predict that the ICEO elastic valve having a thick beam does not work well. Thus, the cilialike ICEO elastic valve is useful in a relatively narrow channel (e.g., $w \leq 100$ μm), while the ICEO rotary valve [12] is useful for a relatively wide channel (e.g., $w \geq 100$ μm). Furthermore, the direct connection between the lower electrode and the conductive elastic beam intrinsically provides larger-ζ potentials and larger flow velocities than the ordinary ICEO structures such as elliptical or circular cylinders, as shown in Fig. 3. Thus, there is much potential for the cilialike ICEO elastic valve to be used in efficient pumps, mixers, etc. In addition, by using the semiconductor process or microelectromechanical-systems technology (similar to Refs. [2,6]), in the future, we can experimentally realize the elastic valve using ICEO, although it might be a challenging problem.

B. Neglect of an unsteady term in the Stokes equation

Because ions diffuse more slowly than vorticity by a factor of $D/\nu = \rho D/\mu \simeq 10^{-3}$, it is customary in microfluidic and colloidal systems to neglect the unsteady term $(\rho\partial \boldsymbol{v}/\partial t)$ in the Stokes equation, as mentioned in Ref. [8]. Here, D $(= 10^{-9}$ m^2/s, for water) and ν $(= \mu/\rho \simeq 10^{-6}$ m^2/s, for water) are the diffusion constant and the dynamic viscosity, respectively. Please note that for a colloidal particle of radius a $(\ll w)$ in an electrolyte, the natural characteristic length l_c and time t_c are the radius a and the ion diffusion time a^2/D, respectively. Thus, the Reynolds number that we should first consider for the vorticity and Navier-Stokes equations concerning the colloidal system is $\text{Re}^{\text{first}} = l_c(l_c/t_c)/\nu = (1/\nu)(l_c^2/t_c) = (1/\nu)(a^2/a^2/D) = D/\nu = 10^{-3}$. That is, the Reynolds number does not depend on the selection of the characteristic length in this case, and it is very small. Further, for the motion of the elastic valve, we need to select d as l_c rather than w, since the slip velocity of the beam edge (V_s^{edge}) of length d (typically, 4 μm) dominates the motion of the valve and the surrounding flow. Furthermore, of course, $V_s^{\text{edge}} (= c_e \epsilon E_0^2/\mu)$ should be selected as a characteristic velocity for the motion of the elastic valve, and the maximum value of V_s^{edge} is approximately 30 mm/s. Thus, the Reynolds number that we should consider second

is $\mathrm{Re}^{\mathrm{second}} = V_s^{\mathrm{edge}} d/\nu \simeq 0.12$ at most, and it is also small enough. Therefore, the neglect of the unsteady term is also justified as a first attempt.

C. Charging time for the edge region

In general, the charging time plays an important role in ICEO phenomena, and two kinds of charging time are well known [20]: the Debye charging time $\tau_D = \lambda_D^2/D$ and the RC charging time $\tau_{RC} = \lambda_D(l_g/2)/D$, where $\lambda_D(= \sqrt{\epsilon kT/2z^2e^2C_0})$ is the Debye screening length, k is the Boltzmann constant, T is the absolute temperature, ze is the ion charge, and C_0 is the bulk ion concentration. Please note that τ_D is often referred to for colloidal particles, while τ_{RC} is often considered for the problems of a parallel electrode whose gap distance is l_g. For our problem, since $L \gg d$, the charging time of the edge region should be estimated by τ_D or $\tau_A = \sqrt{\tau_D \tau_{\mathrm{dif}}} = \lambda_D d/D$ rather than τ_{RC}, where $\tau_{\mathrm{dif}}(= d^2/D)$ is a diffusion time over the edge region. Please note that the capacitance of the edge region of the length d is much smaller than the capacitance of the counter electrode of the length L by the order of d/L. Specifically, if we set $C_0 = 1$ mM, $d = 4$ μm, and $l_g \simeq 50$ μm (as a typical value corresponding to the calculation in Fig. 2), we obtain $\lambda_D \simeq 10$ nm, $\tau_D = 0.1$ μs, $\tau_A = 40$ μs, and $\tau_{RC} = 0.25$ ms. Thus, our calculations are justified since $t_r^{\text{ICEO elastic valve}}$ (approximately 5–10 ms) is much larger than τ_D and τ_A. Further, although we think that the value of τ_{RC} is obviously an overestimation for the edge charging problem, even this worst estimation might be acceptable for the value of $t_r^{\text{ICEO elastic valve}}$ as a first attempt, since our conclusion that $t_r^{\text{ICEO elastic valve}} \sim 5$–10 ms is not changed even if there is a delay time of 0.25 ms.

D. Response time of the ICEO elastic valve

From Figs. 2(e) and 2(f), we consider that the response time of the ICEO elastic valve is about 5–10 ms at $\Delta P = -4$ Pa. However, the response time includes the effect of the pumping function of the elastic valve in the $-x$ direction. That is, at $t = 5$ ms, the forward flow is stopped by the pumping effect as shown in Fig. 2(f); however, the deflection of the beam is not enough to achieve the geometrical closing state as shown in Fig. 2(e). In other words, the geometrical closing time of the ICEO elastic valve is about 10–15 ms at $\Delta P = -4$ Pa, from Fig. 2(e). Thus, the real response frequency of the elastic valve is about 67–100 Hz. Therefore, the response frequency is still high, but it is marvelously comparable to the higher range of the beating frequency of the cilia in nature, since the beating or rotation frequency of the natural cilia (whose typical length is on the order of 10 μm) is 10–100 Hz [21]. Please note that the response frequency of the ICEO valve does not depend on the unit scale of w if the average electric field $E_0(= V_0/w)$ is constant, although we predict that it increases as the value of $\delta^{\mathrm{beam}}/w \simeq (12c_e\epsilon V_0^2/9w^2G)(L_e/d)^3 = (4c_e\epsilon E_0^2/3G)(L_e/d)^3$ increases at $\nu = 0.5$ and $\Delta P = 0$ from Eq. (13).

E. An oscillatory field

Since an ICEO flow velocity is proportional to E_0^2 $[= (V_0/w)^2]$, instead of the dc pulse voltage of a width T_p, we can use an ac applied voltage of the width T_p with a frequency f_{ac} that is smaller than the charging frequency $1/\tau_A$ but larger than $1/T_p$ (i.e., $1/T_p < f_{\mathrm{ac}} < 1/\tau_A$). Further, since the ICEO active closing time and the passive opening time at $\Delta P = +4$ Pa is about 15 and 10 ms, respectively, the maximum beating frequency f_b^{ICEO} of the ICEO valve is about $1/0.025 = 40$ Hz. Of course, there is no relation between this beating frequency and the ac frequency because of the ICEO characteristics. Furthermore, different from the natural cilia, the ICEO valve geometrically propels the same volume of water during active and passive motions; thus, we cannot expect the pumping effect directly from the beating motion. However, because of the asymmetrical structure of the oblique beam, a net ICEO flow in the $-x$ direction generates during the active motion; thus, a pumping function in the $-x$ direction can be expected at $\Delta P = 0$ during the beating motion. Moreover, in general, our proposed numerical method is useful for the study of the natural cilia. However, to use it effectively, we need to model the special beam of the cilia, which is very different from the ordinary elastic beam; i.e., the beam of the cilia works as an elastic beam during the power stroke, whereas it is rather folded during the recovery stroke.

F. The passivation film for the upper electrode

Since the elastic beam is conductive, it is bad for the device if it touches the upper electrode. Thus, we need to use a passivation film for the upper electrodes in practical applications, although we omit the explanation for simplicity. For example, SiO_2 insulation films whose thickness is about 10 nm are needed on the upper electrode to prevent the shortage of the electrical circuit and to avoid the breakdown of the power supply. However, several mechanisms exist to suppress this undesirable contact, although those mechanisms do not work completely to prevent the contact. For example, the reverse torque due to the elasticity of the beam simply increases as the deflection value increases. Further, as shown in Fig. 5(f) in Ref. [12], the ICEO torque on the beam reduces significantly because of the boundary effect as the beam approaches the upper electrode. Thus, even at $\Delta P = 0$, the beam approaches the upper electrode slowly. In addition, at $\Delta P < 0$, the pressure torque that lowers the beam increases because of the increasing projection length in the y direction as the beam approaches the upper electrode; i.e., a forward flow also seems to suppress the contact.

G. The passive valve

Our simple model includes a simple static model for the passive valve at $V_0 = 0$ V, and it clearly predicts that the passive valve closes for a reverse pressure flow at $\Delta P > 0$, whereas the passive valve opens for a forward pressure flow at $\Delta P < 0$, as shown in Figs. 9 and 10. This valving function mainly originates in the movable beam and the difference of the rotational direction of the beam in the fluid, since the Stokes flow is characterized by the relation that $\boldsymbol{u}(\boldsymbol{x}, -\Delta P) = -\boldsymbol{u}(\boldsymbol{x}, +\Delta P)$ if there is no movable portion in the channel. Further, since the closing time of a passive valve is about 10 ms from Fig. 8(d), the closing frequency is about 100 Hz at $\Delta P = +4$ Pa, and the closing frequency does not depend on the unit scale of w if the average pressure gradient $\Delta P/L$ is constant, although it increases as the value of $\delta^{\mathrm{beam}}/w \simeq [\sin^2\theta/6(1+R_o/R_v)](12\Delta P/9G)(L_e/d)^3(L_e/w)$ increases at $\nu = 0.5$ and $V_0 = 0$ from Eq. (13). Here, we neglect the change of the projection length due to the deflection. Furthermore, the contact between the beam and the upper electrode inevitably happens during a closing motion of the passive pressure valve. Different from the active closing motion due to ICEO, the closing torque due to the pressure difference increases as the beam approaches the upper electrodes, although the reverse torque due to the elastic beam increases. Thus, we may need to prepare a thicker passivation film for the passive valve than that for the ICEO valve to prevent the physical damage of the upper electrode.

H. The possibility of a decreasing of the response time in experiments

Although the large flow velocities (approximately 1 mm/s) of the ICEO flows are experimentally observed for distilled water and electrolyte solutions at low ionic concentration (< 10 mM), there is a tendency that ICEO experimental velocities are often smaller than those predicted by the standard theory, and sometimes they are smaller by an order of magnitude, especially for the electrolyte solution at high ionic concentration (> 10 mM) [22]. Thus, there is a possibility that this fact makes the valve move much slower in experiments than predicted in this paper. However, researchers continue to make an effort to clarify the problems; e.g., Pascall and Squires [23] experimentally showed that the contamination of the driving surface provides a natural mechanism for ICEO flow suppression. Thus, for example, in future experiments, we may avoid a decreasing of the response time of ICEO elastic valves by keeping the driving surface clean. Of course, to solve the problem at a practical level, we need to understand the surface phenomena more deeply from the viewpoints of both fundamental physics and engineering.

I. The large deflection problem of the elastic beam

For simplicity, we just consider the linear beam theory of Eq. (13) for the analytical theory in Sec. II C. However, the presented problem is highly complex. In fact, it belongs to a so-called large deflection problem that requires a highly nonlinear beam theory. Thus, we mainly consider the problem based on the boundary-element method that considers the large deflection problem at each time step. Therefore, the discrepancies between the numerical and analytical results in Sec. III are acceptable as a first attempt. For example, as shown in Figs. 5(d) and 11(d), the dependence of x_p on d in the analytical model is not in good agreement with that in the numerical model; i.e., as the value of d increases, the deflection value decreases rapidly in the analytical model, whereas the deflection value decreases slowly in the numerical model. In other words, the elastic beam in the thicker region is much more flexible than the prediction of the linear simple theory. Here, the discrepancy is reasonable if we consider the large deflection of the elastic beam; e.g., in Figs. 5(d) and 11(d), the elastic beam at $d/w = 0.1$ initially might be stiff, but it becomes flexible as the deflection value becomes large, since the cross-section area (or thickness) of the beam also becomes small in the large deflection process.

V. CONCLUSION

In conclusion, we propose an elastic valve using induced-charge electro-osmosis around a conductive elastic beam in water and numerically examine the outstanding valving performance. By multiphysics simulations using an implicit strongly coupled calculation method between a fluid and an elastic structure along with the thin-double-layer approximation, we find that (1) because of the direct connection between the lower electrode and the conductive elastic beam, the typical ζ potential of the edge position of the beam becomes comparable with the applied voltage ($\zeta^{\mathrm{edge}} \simeq V_0$). (2) The typical tangential electric field of the edge position is also very large because of the oblique structure of the beam ($E_s^{\mathrm{edge}} \simeq 4E_0$). (3) The typical maximum slip velocity of the edge position is approximately 30 mm/s, whose value is about 30 times higher than that of an ordinary ICEO flow ($V_s^{\mathrm{edge}} \simeq 30U_c$). (4) The typical closing time of the elastic ICEO valve is about 5–10 ms at $V_0 = 1.19$ V, and it is marvelously short. (5) Further, the oblique beam stops a reverse flow effectively and releases a reverse flow promptly at $E_0 = 0$. We believe that in the future, our device can be used as a promising biomimic actuator, such as a mixer, a pump, etc.

[1] J. M. J. den Toonder and P. R. Onck, Microfluidic manipulation with artificial/bioinspired cilia, Trends Biotechnol. **31**, 85 (2013).

[2] A. R. Shields, B. L. Fiser, B. A. Evans, M. R. Falvo, S. Washburn, and R. Superfine, Biomimetic cilia arrays generate simultaneous pumping and mixing regimes, Proc. Natl. Acad. Sci. U.S.A. **107**, 15670 (2010).

[3] B. A. Evans, A. R. Shields, R. L. Carroll, S. Washburn, M. R. Falvo, and R. Superfine, Magnetically actuated nanorod arrays as biomimetic cilia, Nano Lett. **7**, 1428 (2007).
[4] S. N. Khaderi, M. G. H. M. Baltussen, P. D. Anderson, D. Ioan, J. M. J. den Toonder, and P. R. Onck, Nature-inspired microfluidic propulsion using magnetic actuation, Phys. Rev. E **79**, 046304 (2009).
[5] E. P. Kartalov and S. R. Quake, Microfluidic device reads up to four consecutive base pairs in DNA sequencing-by-synthesis, Nucleic Acids Res. **32**, 2873 (2004).
[6] Jaap den Toonder, Femke Bos, Dick Broer, Laura Filippini, Murray Gillies, Judith de Goede, Titie Mol, Mireille Reijme, Wim Talen, Hans Wilderbeek, Vinayak Khatavkar, and Patrick Anderson, Artificial cilia for active micro-fluidic mixing, Lab Chip **8**, 533 (2008).
[7] M. Z. Bazant and T. M. Squires, Induced-Charge Electrokinetic Phenomena: Theory and Microfluidic Applications, Phys. Rev. Lett. **92**, 066101 (2004).
[8] T. M. Squires and M. Z. Bazant, Induced-charge electro-osmosis, J. Fluid Mech. **509**, 217 (2004).
[9] Todd M. Squires and Martin Z. Bazant, Breaking symmetries in induced-charge electro-osmosis and electrophoresis, J. Fluid Mech. **560**, 65 (2006).
[10] Antonio Ramos, Hywel Morgan, Nicolas G Green, and Antonio Castellanos, {AC} electric-field-induced fluid flow in microelectrodes, J. Colloid Interface Sci. **217**, 420 (1999).
[11] A. Ramos, A. Gonzalez, A. Castellanos, N. G. Green, and H. Morgan, Pumping of liquids with ac voltages applied to asymmetric pairs of microelectrodes, Phys. Rev. E **67**, 056302 (2003).
[12] H. Sugioka, High-speed rotary microvalves in water using hydrodynamic force due to induced-charge electrophoresis, Phys. Rev. E **81**, 036301 (2010).
[13] H. Sugioka, Rotation of a microvalve near conductive electrodes via electrophoresis, Phys. Rev. E **83**, 025302 (R) (2011).
[14] H. Sugioka, Basic analysis of induced-charge electrophoresis using the boundary element method, Colloids Surf A **376**, 102 (2011).
[15] C. Pozrikidis, *Introduction to Theoretical and Computational Fluid Dynamics* (Oxford University Press, New York, 1997).
[16] A. Ranjibaran, Advanced implementation of the boundary element method in elastostatics, Comput. Struct. **55**, 553 (1995).
[17] Xiaosong Zhang and Xiaxian Zhang, Exact integration in the boundary element method for two-dimensional elastostatic problem, Engineering Analysis with Boundary Elements **27**, 987 (2003).
[18] M. C. Fair and J. L. Anderson, Electrophoresis of non-uniformly charged ellipsoidal particles, J. Colloid Interface Sci. **127**, 388 (1989).
[19] Falko Ziebert, Martin Z. Bazant, and David Lacoste, Effective zero-thickness model for a conductive membrane driven by an electric field, Phys. Rev. E **81**, 031912 (2010).
[20] Martin Z. Bazant, Katsuyo Thornton, and Armand Ajdari, Diffuse-charge dynamics in electrochemical systems, Phys. Rev. E **70**, 021506 (2004).
[21] Vinayak V. Khatavkar, Patrick D. Anderson, Jaap M. J. den Toonder, and Han E. H. Meijer, Active micromixer based on artificial cilia, Phys. Fluids **19**, 083605 (2007).
[22] Martin Z. Bazant, Mustafa Sabri Kilic, Brian D. Storey, and Armand Ajdari, Towards an understanding of induced-charge electrokinetics at large applied voltages in concentrated solutions, Adv. Colloid Interface Sci. **152**, 48 (2009).
[23] Andrew J. Pascall and Todd M. Squires, Induced Charge Electro-Osmosis over Controllably Contaminated Electrodes, Phys. Rev. Lett. **104**, 088301 (2010).